batteries

MDPI

Review

Polycyclic Aromatic Hydrocarbon-Enabled Wet Chemical Prelithiation and Presodiation for Batteries

Yu-Sheng Su [1,2,*] and Jeng-Kuei Chang [3,*]

[1] International College of Semiconductor Technology, National Yang Ming Chiao Tung University, 1001 University Road, Hsinchu 30010, Taiwan
[2] Industry Academia Innovation School, National Yang Ming Chiao Tung University, 1001 University Road, Hsinchu 30010, Taiwan
[3] Department of Materials Science and Engineering, National Yang Ming Chiao Tung University, 1001 University Road, Hsinchu 30010, Taiwan
* Correspondence: yushengsu@nycu.edu.tw (Y.-S.S.); jkchang@nycu.edu.tw (J.-K.C.)

Abstract: The current mainstream energy storage systems are in urgent need of performance improvements to meet novel application requirements. In pursuit of a higher energy density in Li-ion and Na-ion batteries, the conventional electrode materials have reached the upper limit of their theoretical specific capacities. Hence, facile methods of reducing irreversible lithium-ion/sodium-ion loss are developed to further boost the battery energy density. Herein, we review studies that use polycyclic aromatic hydrocarbons for wet chemical prelithiation and presodiation. The molecular structures of arenes and solvents used for solution-based prelithiation/presodiation have a substantial impact on the prelithiation/presodiation power and effectiveness. Multiple reports have already shown excellent initial Coulombic efficiency and streamlined processes by using this type of wet chemical prelithiation/presodiation strategy. This review article will cover how to select appropriate polycyclic aromatic hydrocarbon prelithiation/presodiation reagents for various materials/electrodes and provide possible directions and guidelines for future works.

Keywords: Li-ion battery; Na-ion battery; initial Coulombic efficiency; anode; cathode; arene; naphthalene; biphenyl; 9,9-dimethylfluorene

Citation: Su, Y.-S.; Chang, J.-K. Polycyclic Aromatic Hydrocarbon-Enabled Wet Chemical Prelithiation and Presodiation for Batteries. *Batteries* **2022**, *8*, 99. https://doi.org/10.3390/batteries8080099

Academic Editor: Matthieu Dubarry

Received: 26 July 2022
Accepted: 17 August 2022
Published: 19 August 2022

1. Introduction

Li-ion and Na-ion batteries are leading a new wave of the industrial revolution. After dominating the market of portable consumer electronics, new battery technologies now aim at supplying power to much bigger devices, such as grid-scale energy storage and vehicle electrification [1–5]. To significantly increase the energy density of batteries, replacing traditional electrode materials with next generation anode/cathode materials has yielded many remarkable results in academia research [6–10]. However, there are still many performance and manufacturing gaps that need to be bridged until these state-of-the-art technologies can be adopted in the battery industry, and the progress is not fast enough to keep up with actual developmental needs for new technologies. In this regard, prelithiation/presodiation procedures are favorable for a quick energy boost with the same battery chemistry [11–14].

A typical scenario comparing Li-ion and Na-ion cells without and with prelithiation and presodiation is depicted in Figure 1. Before formation cycles, lithium/sodium ions are stored at the cathode side with a specific capacity of Q_c in a conventional cell. During the first charge, alkali metal ions migrate to the anode side, but some of them are consumed irreversibly, whereas the rest of the ions are stored in the anode ($Q_a = Q_c - IRR$). The irreversible capacity (IRR) mainly results from the solid–electrolyte interface (SEI) formed on the surface of anode, which is an inevitable process to secure anode cycling stability due to the protection of SEI film [15–17]. A study by Winter's group pointed out that the

major part of irreversible capacity from the $LiNi_{1/3}Co_{1/3}Mn_{1/3}O_2$ (NCM) cathode can be recoverable by adjusting the discharge (lithiation) setting with a constant voltage step since the active ion loss is impeded kinetically but not thermodynamically [18]. Thus, the *IRR* loss here is derived mostly from the anode SEI formation, lithium ions that are unfavorably trapped in the structure, and unwanted electrolyte decomposition reactions. After the first discharge, the ions in the anode move to the cathode to complete the reversible electrochemical reaction ($Q_{rev} \approx Q_a = Q_c - IRR$). To compensate for the alkali ion loss during the first cycle, prelithiation/presodiation can be used. Additional active ions are introduced into the battery cell before the formation cycle (shown as the *IRR* block in green). In this case, the alkali ions in the cathode can be fully utilized when transporting to the anode during the first charge ($Q'_a = Q_c$), and thereby the reversible capacity of the prelithiated/presodiated cell is deemed as its maximum ($Q'_{rev} \approx Q'_a = Q_c$). After effective prelithiation/presodiation, all the active lithium or sodium ions are conserved for reversible redox reactions rather than consumed for anode SEI formation, and the anode and cathode capacities can be perfectly utilized to store active ions and then achieve a maximal energy density.

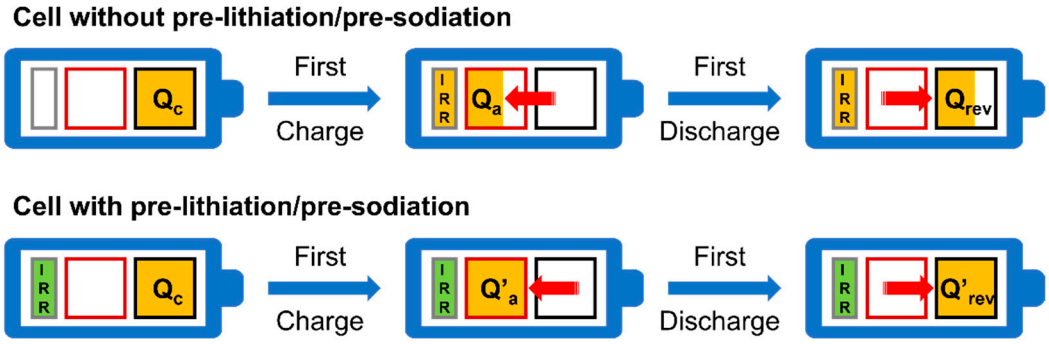

Figure 1. Schematic drawing illustrating how the reversible capacity changes in cells without and with prelithiation/presodiation during the formation cycle. Q_c: initial cathode specific capacity; Q_a and Q'_a: available anode capacity after the first charge; Q_{rev} and Q'_{rev}: reversible capacity after the first discharge.

Many prelithiation/presodiation methods for battery systems have been developed such as wet chemical, molten alkali metal, in situ and ex situ electrochemical, short-circuiting, and alkali metal additions, which are summarized in Table 1. Most of these prelithiation/presodiation techniques utilize pure alkali metal in the form of foil or powder. A unique commercial metallic lithium product called SLMP (stabilized lithium metal powder) was frequently used in the prelithiation of anode in Li-ion batteries for better handling [19–21]. With an external Li_2CO_3 coating layer, SLMP exhibits excellent dry-air stability, outperforming other pristine metallic lithium sources. Molten alkali metal is a prelithiation/presodiation method that is not easily used for electrode-level operations, and a raised processing temperature is required to liquify the alkali metals, making this approach relatively unsafe and questionable for large-scale manufacturing [22,23]. On the other hand, wet chemical and direct alkali metal addition routes are both capable of being applied in either material- or electrode-level prelithiation/presodiation. The binder/solvent system must be specially selected to be compatible with highly reactive prelithiated/presodiated materials. There are two types of electrochemical prelithiation/presodiation means, which are via in situ or ex situ courses, and both are controlled by an external circuit. The in situ electrochemical method is conducted by introducing an additional layer of alkali metal foil into the cell with porous current collectors, and then connecting the metal electrode with the anode to initiate the process [24]. The ex situ electrochemical approach is more complicated, requiring another electrochemical bath setup and implementing prelithiation/presodiation before battery reassembly [24]. If the prelithiation/presodiation process is accomplished via direct alkali metal contact (e.g., spreading SLMP, short-circuiting, etc.),

external pressure has to be applied to activate the reaction. The protective film on SLMP can be cracked by the applied pressure to trigger the process, and an enhanced alkali metal/electrode contact leads to homogeneous and controllable ion distribution [11–13,22]. When solvents or electrolytes are used for the prelithiation/presodiation in wet chemical, electrochemical, and short-circuiting methods, a following washing step might be necessary to eliminate residual reagents and byproducts. Last but not least, scalability is always the key determining whether the process has commercial value. Most electrode-level prelithiation/presodiation processes are compatible with roll-to-roll production design [25–33], indicating great potential for scaled-up manufacturing in the future. Among these various prelithiation/presodiation selections, the wet chemical method shows the flexibility to be used in both materials and electrodes, possesses minimal processing requirements (room temperature operation; no external circuit and pressure needed), and can be applied to a roll-to-roll and cost-effective battery production line as an add-on prelithiation/presodiation process.

Table 1. Summary of various prelithiation and presodiation techniques and classifications for battery applications.

Methods	Alkali Ion Sources	Material or Electrode Level	Processing Temperature	External Circuit	Pressure Activation	Washing Step	Roll-to-Roll Capability
Wet Chemical	Li/Na Containing Compounds	Both	RT	NR	NR	Maybe	Yes
Molten Alkali Metal	Li/Na Metal	Material	Above MP	NR	NR	NR	NA
Electrochemical	Li/Na Metal Foil	Electrode	RT	Required	NR	Maybe	Yes
Short-circuiting	Li/Na Metal Foil	Electrode	RT	NR	Required	Maybe	Yes
Alkali Metal Addition	Li/Na Metal Foil/Powder	Both	RT	NR	Required	NR	Yes

RT: room temperature; MP: melting point; NR: not required; NA: not applicable.

2. Features of Polycyclic Aromatic Hydrocarbon-Enabled Wet Chemical Prelithiation/Presodiation

Early chemical prelithiation methods utilized a highly flammable and reactive chemical liquid *n*-butyl lithium (*n*-BuLi) to reduce the *IRR* of negative and positive electrodes [34,35]. However, the prelithiation reagent *n*-BuLi has a relatively high redox potential (≈1 V vs. Li/Li^+) and spontaneously combusts in air, making it unfavorable for commercialization due to its poor prelithiation power and safety. Tabuchi et al. developed another type of prelithiation reagent adopting a lithium–organic complex solution by dissolving metallic lithium and naphthalene (Naph) in butyl methyl ether (BME) or dimethoxyethane (DME) [36,37]. In fact, other polycyclic aromatic hydrocarbons (PAHs or arenes), such as biphenyl (BP) and 9,9-dimethylfluorene (DiMF), can replace naphthalene to make PAH complex solutions with alkali metals [38,39]. The PAH compounds form radical anions when an alkali metal is presented, and then a PAH complex molecule is formed containing alkali metal ions. When electrodes/materials react with the PAH complex solution, the radical PAH anion donates its electron and the alkali metal ion reduces, resulting in the completion of prelithiation/presodiation. Since the electron affinity of each PAH is different [39], individual PAH complexes shows differences in terms of prelithiation/presodiation power (i.e., different redox potentials) that will be discussed in the next section. Due to the much lower redox potential and process-friendly solution-type prelithiation/presodiation procedures, a lot of related studies using PAH complex solutions have been published since 2019 [25,32,33,40–62].

The prelithiation potential of typical Li-PAH radical anions can be seen in Figure 2. Three main lithium–organic reagents are $Li^+[Naph]^-$, $Li^+[BP]^-$, and $Li^+[DiMF]^-$, which are ranked from high to low in terms of lithiation/de-lithiation potential [40]. $Li^+[DiMF]^-$ offers better reduction power than that of $Li^+[Naph]^-$ and $Li^+[BP]^-$ for deep anode prelithiation. These arenes with simple structures are common organic compounds produced in industry, which can guarantee scalable and low-cost production. During the prelithiation

process, the preparation and handling of Li-PAH complex solutions are quite safe due to their chemical stability. By controlling the concentration of reagents, reaction time, and temperature, precise, uniform, and highly efficient prelithiation can be achieved. The outcome of PAH-enabled prelithiation/presodiation is a battery with a near-perfect initial Coulombic efficiency (ICE), along with a preformed protective SEI layer on the anode surface that can promote cycle stability.

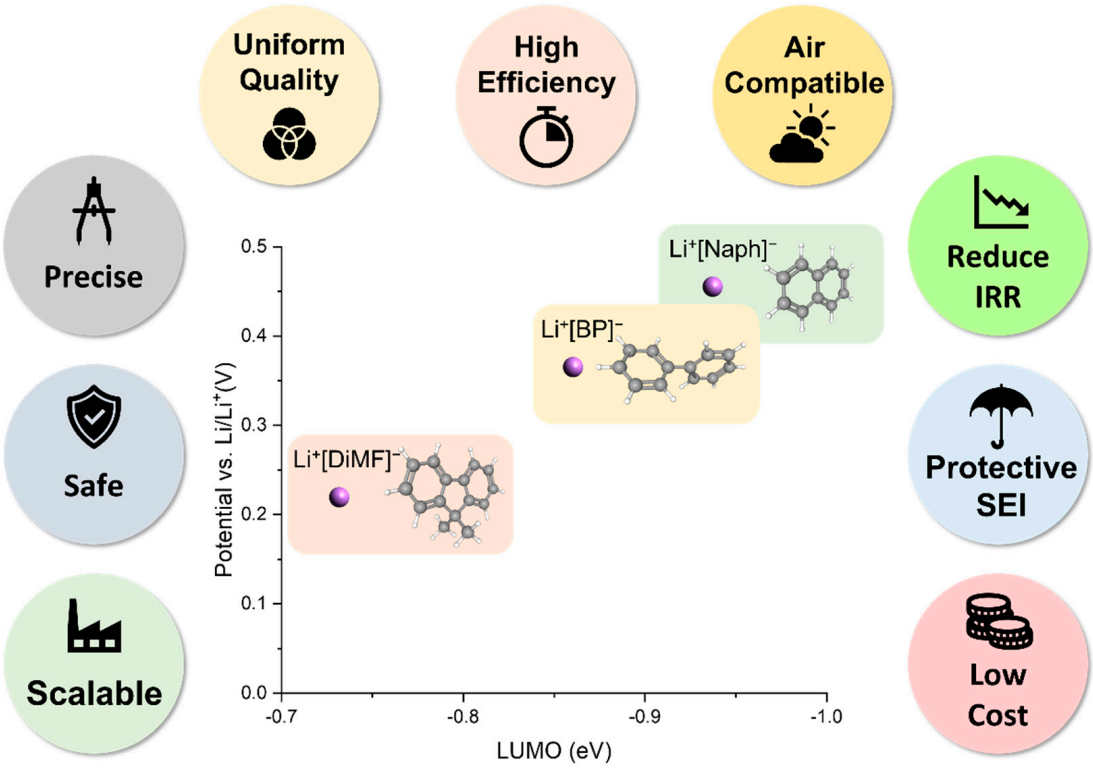

Figure 2. Schematic drawing illustrating the advantages of using PAH-based prelithiation reagents for wet chemical prelithiation.

It is worth noting that a couple of reports indicating the ambient-air processibility of Li-PAH complex solutions and prelithiated anodes, displayed in Figure 3. Qu et al. found that a higher concentration of Li-BP in tetrahydrofuran (THF) gave good air stability for at least two weeks (Figure 3a) [62]. Prelithiation reagents such as Li-P powder, Li-Sn powder, and a low-concentration Li-BP/THF (0.01 M) solution rapidly changed color after the exposure under ambient atmosphere [62]. The 1 M Li-BP/THF complex solution also showed great stability and still maintained its dark-blue color when being stirred in air, which turned colorless when water was added (Figure 3b), highlighting that the solution was still active until it reacted with water [62]. The authors claimed that the Li-BP/THF complex solution was functionally reactive even after 9 days of storage, yielding similarly effective prelithiation results in either glovebox or ambient air [62]. They also proposed that electrode prelithiation can be carried out under ambient air. After the completion of prelithiation using Li-BP/THF, the residual complex does not need to be removed by electrode washing, and the Li-BP layer can therefore protect the prelithiated electrode (Figure 3c). The additional BP remaining on the electrode can be removed later by its dissolution in carbonate-based electrolytes [62]. Wang et al. utilized a Li-DiMF complex solution to prelithiate aluminum foil to form LiAl alloy with an alumina-containing artificial SEI layer [40]. Figure 3d exhibits the air stability of different lithiated anodes (c-LiAl: wet chemically prelithiated Al; e-LiAl: electrochemically prelithiated Al; e-Li/Cu: electrochemically deposited Li on Cu). After 30 min of exposure to air, only e-Li/Cu showed significant oxidation, verified by the color change. In terms of capacity retention,

the Li-DiMF prelithiated c-LiAl, at over 91% of the initial capacity, which significantly outperformed the other two electrode samples lithiated via the electrochemical method [40]. The preformed SEI generated during wet chemical prelithiation plays an important role in resisting the corrosion induced by oxygen and moisture. Figure 3e shows another example of dry-air-stable prelithiated electrodes processed by tailored Li-BP complex solutions [32]. The SiO_x electrode lost some ICE after 5 min of dry-air exposure, but stabilized thereafter and still gave more than 100% of ICE. Additionally, no significant overpotential was found in the electrode after exposure to dry air [32]. These process-friendly features make the wet chemical PAH-based prelithiation/presodiation potential candidates to be integrated into the large-scale battery cell manufacturing process, which is always conducted in dry rooms.

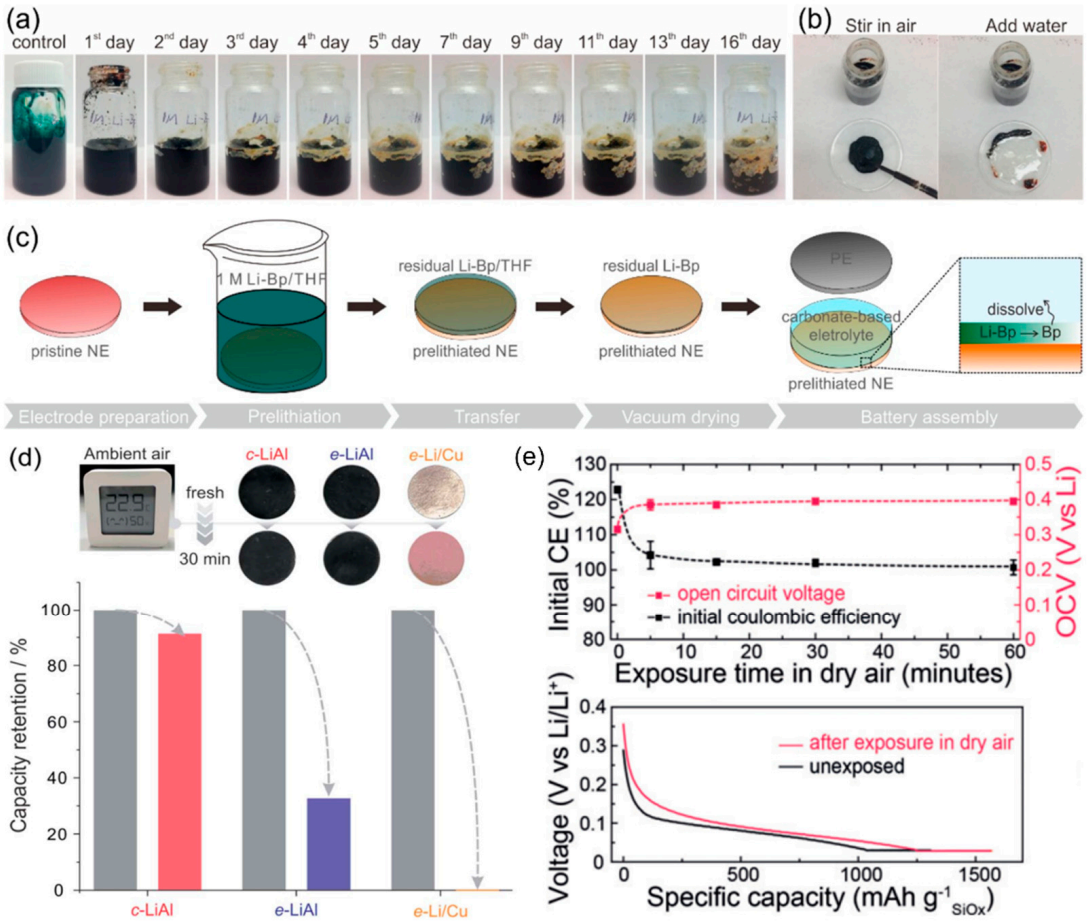

Figure 3. (**a**) Photos of the 1 M Li-Bp/THF complex solution exposed to ambient air for different durations. (**b**) Photos of the 1 M Li-Bp/THF complex solution under stirring in ambient air or after adding water. (**c**) Schematic illustration showing the prelithiation procedure in ambient air. Reproduced with permission from ref. [62]. Copyright 2019, ACS Publications. (**d**) Capacity retentions of c-LiAl (chemically prelithiated Al by Li-DiMF), e-LiAl (electrochemically prelithiated Al), and e-Li/Cu (electrochemically deposited Li on Cu) after 30 min of exposure to ambient air. Reproduced with permission from ref. [40]. Copyright 2020, The Royal Society of Chemistry. (**e**) Initial Coulombic efficiency (black, top), OCV (pink, top), and voltage profiles (bottom) of the prelithiated SiO_x anode exposed to dry air for different durations. Reproduced with permission from ref. [32]. Copyright 2020, Wiley-VCH.

3. Adjusting Prelithiation/Presodiation Power and Rate of PAH Complex Solutions

Several research groups have identified the redox potentials of various PAH radical anions, predominantly for Li-ion battery applications. Wang et al. screened various PAH molecules to obtain a low enough redox potential and a high enough lowest unoccupied molecular orbital (LUMO) energy in order to prelithiate Al foil (Figure 4a) [40]. DiMF, calculated to have a LUMO energy of −0.758 eV using density functional theory (DFT), was found to have a quasi-reversible redox couple with a redox potential of 0.22 V vs. Li/Li^+, showing the best prelithiation power compared to Naph, BP, and other PAH with more aromatic rings [40]. Lee et al. modified the molecular structures of BP by introducing electron-donating methyl groups into the benzene ring, and the electron density can be increased while the electron affinity and reduction potential are decreased [32]. Once methyl groups are added to the BP molecule, all derivatives exhibit a lower redox potential and a higher LUMO energy (Figure 4b) [32]. Either one methyl substitution at the ortho position (2-methyl BP; blue molecule in Figure 4b) or four methyl groups at both the meta and para positions (3,3′,4,4′-tetramethyl BP; orange molecule in Figure 4b) offer a great prelithiation power close to 0.1 V vs. Li/Li^+, enabling an effective prelithiation of Si/SiO_x anodes [32]. Instead of grafting methyl groups on BP, Qian et al. engineered the substituent of naphthalene with different functional groups onto the alpha position to tune the prelithiation power [53]. Figure 4c lists a series of Li-Naph molecules, which offer different prelithiation power that can be distinguished from their unique cyclic voltammetry curves [53]. Among them, 1-cyanonaphthalene (CNaph) not only improves the ICE of SiO electrode to over 100%, but also promotes the formation of a rectified SEI containing nitrile-rich outer layer and an inorganic LiF-rich inner layer [53]. However, not all the modified PAH molecules can perform prelithiation/presodiation. After reacting with metallic lithium, 2-fluorobiphenyl (BP grafted with a fluorine atom), even possessing suitable LUMO energy (Figure 4d), does not have much prelithiation power because LiF and defluoriated BP are the dominated products rather than reactive BP-based radical anions [54]. Although some PAH complexes with a higher redox potential (>0.8 V vs. Li/Li^+) cannot be used to prelithiate anodes, they are good relithiation reagents for spent cathodes with deficient lithium ions [52]. Pyrene (Py) and perylene (Per) can regenerate recycled $LiFePO_4$ (LFP) and $LiCoO_2$ (LCO) cathodes, respectively, since they both have sufficiently higher redox potentials to avoid cathode decomposition (Figure 4e) [52]. As a result, the prelithiation/presodiation potential of PAH radical anions is flexibly tunable to be applied in a variety of situations, making them facile and universal prelithiation/presodiation reagents.

In addition to the PAHs with modified molecular structures, the solvent in the PAH complex solution plays a critical role in electrochemical reactions during prelithiation/presodiation. DME and THF are frequently used solvents to dissolve PAH compounds along with alkali metals. Ai et al. adopted a modified THF solvent, 2-methyl tetrahydrofuran, with a higher tendency to donate electrons (2-Me-THF), yielding better results with regard to graphite anode wet chemical prelithiation [55]. By investigating DFT calculations, assuming one lithium ion coordinating with two oxygen atoms of the solvent, Li-BP in 2-Me-THF gives the largest highest occupied molecular energy (HOMO), which means the lowest reduction potential in comparison with other Li-BP-solvent complexes (Figure 5a) [55]. The Li-BP/2-Me-THF system offers a much lower redox potential (0.08 V) than those of Li-BP/THF (0.26 V) and Li-BP/DME (0.30 V), indicating a better lithiating power for anode materials with a low redox potential (e.g., graphite) [55]. Wu et al. discovered that Li-PAH solution kinetically changes its conductivity as the duration of the lithiation increases (Figure 5b) [54]. In the beginning, 4,4-dimethyl BP (4,4-DMBP) is dissolved in THF, followed by the addition of metallic lithium to form the complex solution. Then, the THF solvent molecules solvate lithium ions to form $Li(THF)_n^+$, and the radical anions $(4,4\text{-DMBP})^{\bullet-}$ are simultaneously formed by accepting electrons from the lithium [54]. Plenty of solvent-separated ion pairs (SSIPs) and contact ion pairs (CIPs) generate after this stage, leading to a quick conductivity boost. Afterwards, the conductivity of solution gradually decays due to the association of $Li(THF)_n^+$ with $(4,4\text{-DMBP})^{\bullet-}$ as aggregates [54].

The authors found that the associated active species may have a higher prelithiation activity than dissociated ion pairs, but the prelithiation uniformity of the aggregates, formed by resting the PAH complex solution for a longer time, is not comparable to the freshly made one [54]. The changing conductivity of the Li-PAH complex solution implies that the lithiating power could change with the lithiation time, making the prelithiation control somewhat challenging. Lee et al. examined various solvents in the PAH complex solutions and ranked their solvation power as tetrahydropyran (THP) < 2-Me-THF < THF < DME [56,63,64]. When a strong solvent (e.g., DME) is used, the formation of SSIPs dominates, leading to the poor desolvation of lithium ions and thereby the co-intercalation of solvent molecules can occur [56]. This behavior makes DME incapable of being used to prelithiate graphite anodes due to the solvated lithium ions ($Li(DME)_n^+$) exfoliating and degrading the graphite structure [55,56,65,66]. Figure 5c,d compare the energies between BP decoordination and solvent molecule desolvation in different solvent systems. When there are two DME solvent molecules around $Li^+(BP)^{\bullet-}$, the formation of free $(BP)^{\bullet-}$ anions and solvated $Li(DME)_2^+$ is favored (shown as a pink box in Figure 5c), generating unwanted SSIPs and resulting in solvent co-intercalation [56]. On the contrary, in a weak solvent system such as THP, the desolvation of THP dominates the process and CIPs are major products no matter how many solvent molecules are surrounding the lithium ion (Figure 5d) [56]. As a result, an appropriate solvent selection for the PAH complex solution can adjust the prelithiation/presodiation power, activity, uniformity, and solvation/coordination behaviors for better wet chemical prelithiation/presodiation performance.

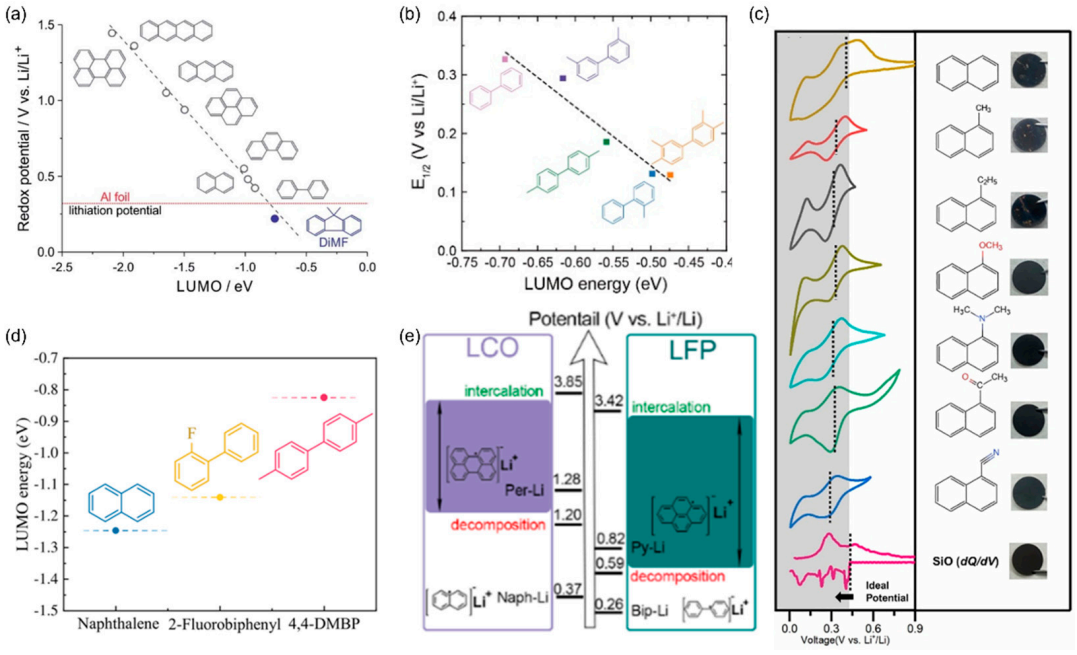

Figure 4. (**a**) The correlation between the redox potentials and LUMO energies of PAH molecules. Reproduced with permission from ref. [40]. Copyright 2020, The Royal Society of Chemistry. (**b**) The correlation between the redox potentials ($E_{1/2}$) and LUMO energies of BP derivatives. Reproduced with permission from ref. [32]. Copyright 2020, Wiley-VCH. (**c**) Cyclic voltammograms for Li-Naph derivatives in 1.0 M $LiPF_6$/THF, differential capacity curves for the SiO electrode, and photos of the prelithiated SiO electrodes immersed in 0.2 M Li-Naph derivative systems for 2 h. Reproduced with permission from ref. [53]. Copyright 2022, Elsevier. (**d**) LUMO energies of PAH derivatives. Reproduced with permission from ref. [54]. Copyright 2021, ACS Publications. (**e**) The redox potentials of various Li-PAH complexes in comparison with the intercalation/decomposition potentials of LFP and LCO cathodes. Reproduced with permission from ref. [52]. Copyright 2021, ACS Publications.

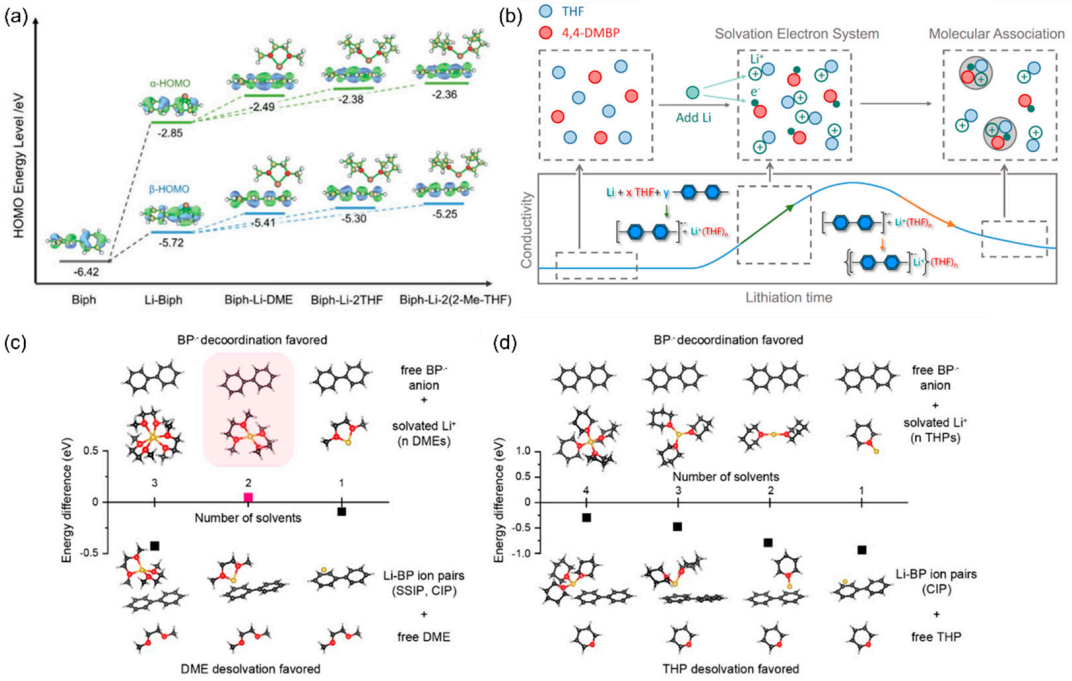

Figure 5. (**a**) Geometrical configurations and HOMO energies of the Li–Biph(BP) in DME, THF, and 2-Me-THF. Reproduced with permission from ref. [55]. Copyright 2021, Wiley-VCH. (**b**) Schematic illustration showing the formation and evolution of lithium radical anions and the corresponding conductivity change in the solution during lithiation. Reproduced with permission from ref. [54]. Copyright 2021, ACS Publications. Prediction of Li-ion desolvation paths by evaluating the thermodynamic stability of possible ion-pair intermediates (**c**) in the strong solvent DME and (**d**) in the weak solvent THP using DFT calculations. Reproduced with permission from ref. [56]. Copyright 2021, ACS Publications.

4. Anode Prelithiation Using PAH Complex Solutions

Due to the high reducing ability of the anode in lithium-ion batteries, the SEI generated by the decomposition of electrolyte consumes a lot of active lithium. This makes anode prelithiation very attractive to efficiently improve the energy density of battery. Most of the prelithiation studies using PAH complex solutions focused on raising the ICE of anode to close or over 100%, summarized in Table 2. Not only conventional graphite anodes [55,56], but also high-power hard carbon anodes [41,44,54] and high-capacity silicon monoxide anodes [32,33,36,43,53,56] (both ICE < 80%) have been demonstrated to be compatible for the prelithiation with various lithium arene radical anions. Carbon-based anodes can be prelithiated within a very short time, ranging from just 0.5 to 5 min. SiO_x anodes with a higher capacity (>1000 mAh g^{-1}) would require a longer duration of prelithiation (10–30 min) to compensate for their large IRR. Some carbon-enhanced composite anodes such as tin oxide [42] and phosphorus [45,62] also showed much better ICEs after adopting 1 M Li-BP/THF as the prelithiation reagent. Generally, the reaction time was manipulated to control the level of prelithiation in previous reports. There have been no systematical studies of how the concentration and Li/PAH ratio of complex solutions may affect the prelithiation power and solution stability, which require further investigation. Recent research mainly used the concentration from 0.2 M to 1 M and the Li/PAH ratio from 1 to 8 to prepare the Li-PAH complex solutions, but how these recipes were designed remains unknown.

Table 2. Summary of prelithiated anode performance adopting various Li-PAH complexes.

Anode	Li-PAH Complex	Prelithiation Time (min)	Reversible Capacity (mAh g^{-1})	ICE before Prelithiation	ICE after Prelithiation	Reference
Graphite	1 M Li-BP/2-Me-THF	5	365	84.4%	98.8%	[55]
Graphite	0.2 M Li_4-BP/2-Me-THF	2	354	90.4%	110%	[56]
Graphite/Si		1	583	83.2%	98.6%	
Graphite/SiO_x		1	911	74.1%	103.2%	
Hard Carbon	1 M Li_4-4,4-DMBP/THF	0.5	≈290	78.7%	100%	[54]
Hard Carbon	0.5 M Li-Naph/DME	4	≈405	75.5%	99.5%	[41]
Hard Carbon	1 M Li-BP/THF	0.5 2	295 (lithiation first) 321 (delithiation first)	79.2%	104.4% 91.2%	[44]
$Li_4Ti_5O_{12}$	0.25 M Li-Naph/BME	180	161	NA	NA	[37]
SiO	0.25 M Li-Naph/BME	4320	670	NA	NA	[36]
SiO	0.2 M Li_8-CNaph/THF	30	≈1700	77%	107.6%	[53]
SiO_x	0.5 M Li_4-4,4-DMBP/DME	30	1587	57%	107%	[32]
Graphene/SiO	1 M Li-DiMF/THF	10	≈1050	71.2%	87.1%	[33]
Carbon/SiO_x	1 M Li-BP/THF	NA	1349	75.6%	87.3%	[43]
Carbon/SnO_2	1 M Li-BP/THF	5	870	45%	90%	[42]
Carbon/P	1 M Li-BP/THF	10	≈1200	74%	94%	[62]

NA: not applicable.

An added benefit of using the PAH-enabled wet chemical prelithiation is that the preformed SEI may be more uniform, more ionically conductive, mechanically stronger, and chemically more stable than the in situ-formed SEI during the formation cycles. Figure 6a,b compare the SEI formed in the pristine and prelithiated hard carbon anodes after the initial cycle [41]. The prelithiated anode can promote the growth of a thinner and denser SEI, where LiF builds up after the preformed Li-OR-rich SEI reacts with the electrolyte during the first lithiation reaction [41]. Wu et al. discovered that the Li-PAH complex solution prepared in a shorter time (10 min vs. 60 min) has a slower prelithiation rate (80 s vs. 60 s) but can generate a more homogeneous preformed SEI layer, leading to smaller overpotential and electrochemical impedance (Figure 6c) [54]. Qu et al. compared two different procedures (lithiation first vs. delithiation first) after cell assembly for the Li-PAH prelithiated hard carbon anodes [44]. They proposed that the anode SEI be chemically formed under the lithiation-first procedure and electrochemically formed under the delithiation-first procedure. Although the reversible capacity was higher with the delithiation-first setting, the cell gave a lower ICE and never reached over 92.6% (Figure 6d) [44]. In contrast, when the prelithiated anode was first lithiated in the cell, the ICE can be lifted up to 186.8%. Nevertheless, both methods exhibited similar cycle stability values. Guo et al. made a head-to-head comparison between the SLMP and Li-BP prelithiated SiO_x anodes, as shown in Figure 6e, where the latter outperformed the former in terms of capacity retention [43]. Figure 6f,g display the cross-section of the SLMP and Li-BP prelithiated SiO_x anodes after cycling, respectively. A more homogeneous Li_xSiO_y distribution, the major lithiated product of SiO_x [67], can be found in the Li-BP prelithiated sample, resulting in better structural stability under repeated swelling and shrinkage during cycling. Consequently, the PAH-enabled wet chemical prelithiation can not only increase the ICE of anodes, but also modify the composition and uniformity of artificial SEI for better electrochemical performance. The mechanical properties of the SEI layer need to be investigated in detail in the future to further confirm which prelithiation method could produce a stronger SEI on the anode.

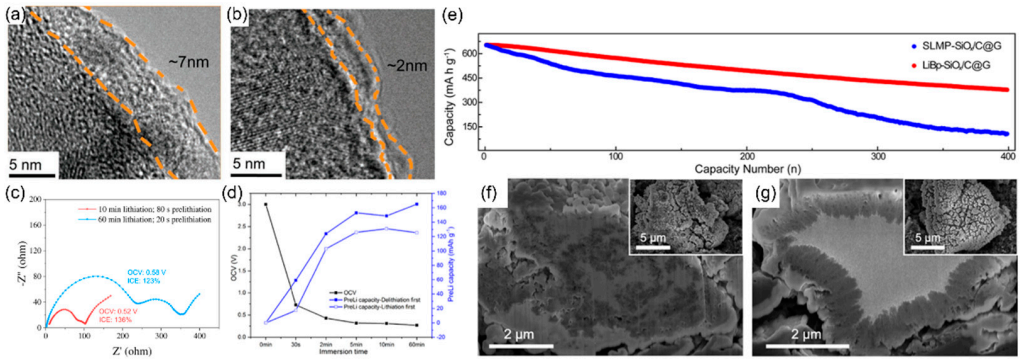

Figure 6. TEM images of (**a**) pristine hard carbon anode and (**b**) prelithiated hard carbon anode after initial cycle. Reproduced with permission from ref. [41]. Copyright 2020, Wiley-VCH. (**c**) Electrochemical impedance spectra of two half-cells assembled with hard carbon anodes prelithiated by Li-DMBP (10 min) and Li-DMBP (60 min), with a similar degree of prelithiation. Reproduced with permission from ref. [54]. Copyright 2021, ACS Publications. (**d**) OCV values and prelithiation capacities of hard carbon anodes with different procedures. Reproduced with permission from ref. [44]. Copyright 2020, ACS Publications. (**e**) Cycling performance of the Li-BP and SLMP prelithiated SiO_x anodes. Top-view and cross-sectional SEM images of the (**f**) SLMP prelithiated and (**g**) Li-BP prelithiated anodes after 200 cycles. Reproduced with permission from ref. [43]. Copyright 2020, ACS Publications.

5. Cathode Prelithiation Using PAH Complex Solutions

Other than anode prelithiation, the strategy of utilizing prelithiated cathodes can enhance the battery energy density as well by compensating the active lithium loss from the anode. Sun et al. used a Li-Naph/THF system to create a core–shell structure for LCO cathode materials [47]. After prelithiation, the outer nanoshell of $LiCoO_2$ is converted into Li_2O/Co, which offers additional delithiation capacity and forms a Co_3O_4 shell during charging (Figure 7a) [47]. Qian et al. tried to develop a suitable PAH complex solution to relithiate the spent LCO and LFP cathode materials [52]. Nevertheless, using Li-Naph (E_{redox} = 0.37 V vs. Li/Li^+) will decompose both LCO (E_{redox} = 1.20 V vs. Li/Li^+) and LFP (E_{redox} = 0.59 V vs. Li/Li^+), leading to irreversible phase change (Figure 7b). Therefore, Li-Per (E_{redox} = 1.28 V vs. Li/Li^+) and Li-Py (E_{redox} = 0.82 V vs. Li/Li^+) are good candidates to lithiate LCO and LFP, respectively, without damaging the cathode material. Figure 7c illustrates how this mild wet chemical relithiation process can restore the aged LFP cathode material structure with lithium loss. A Li-enriched gradient interface (~20 nm) can be generated on Ni-rich layered oxide cathode materials through prelithiation in Li-Naph/THF [50]. Figure 7d shows that a higher concentration of lithium can be found close to the material surface, where more reduced nickel (Ni^{2+}) is generated simultaneously. This Li-rich cathode structure can supply extra lithium to resolve the IRR issue from the anode and thereby boost the energy density of the full cell.

Most conversion-type cathode materials are Li-free, so making use of them is very challenging [68,69]. However, in order to improve the energy density of batteries, it is necessary to use new cathode materials to replace traditional intercalation-type cathode materials. In this field, the excellent energy density and low cost of sulfur cathodes have attracted tremendous attention in recent years [70,71]. Although the conversion cathode can pair with metallic lithium to make a full cell, a prelithiated cathode could be used with a lithium-free anode to build a high-energy-density battery, leading to a higher possibility of new battery chemistries. In the past, active Li_2S or lithium polysulfides (Li_2S_x; $6 \leq x \leq 8$) for Li-S batteries were obtained commercially or made by co-dissolving Li_2S and sulfur in solvents [72,73]. Figure 7e exhibits another way to synthesize Li_2S by utilizing a Li-Naph complex solution to prelithiate sulfur [74]. For constructing a Li-S cell without pairing with an unstable metallic lithium metal anode, sulfurized polyacrylonitrile (S-PAN) cathode materials are considered a better alternative to sulfur/carbon composites

because of their compatibility with carbonate-based electrolytes [75–77]. Shen et al. built a lithium metal-free Si/S battery by prelithiating both the silicon anode and S-PAN cathode (Figure 7f) [48]. A high specific energy (710 Wh kg^{-1}) and ICE (93.45%) were obtained in this cell configuration design adopting a Li-Naph complex solution [48]. Zuo et al. used the prelithiated product of S-PAN, Li_2S-PAN, as the prelithiation reagent to prelithiate LFP electrodes, as illustrated in Figure 7g [46]. Here, Li-BP cannot be directly used to prelithiate LFP due to its low working voltage, which may result in LFP decomposition, as described in the previous paragraph [52].

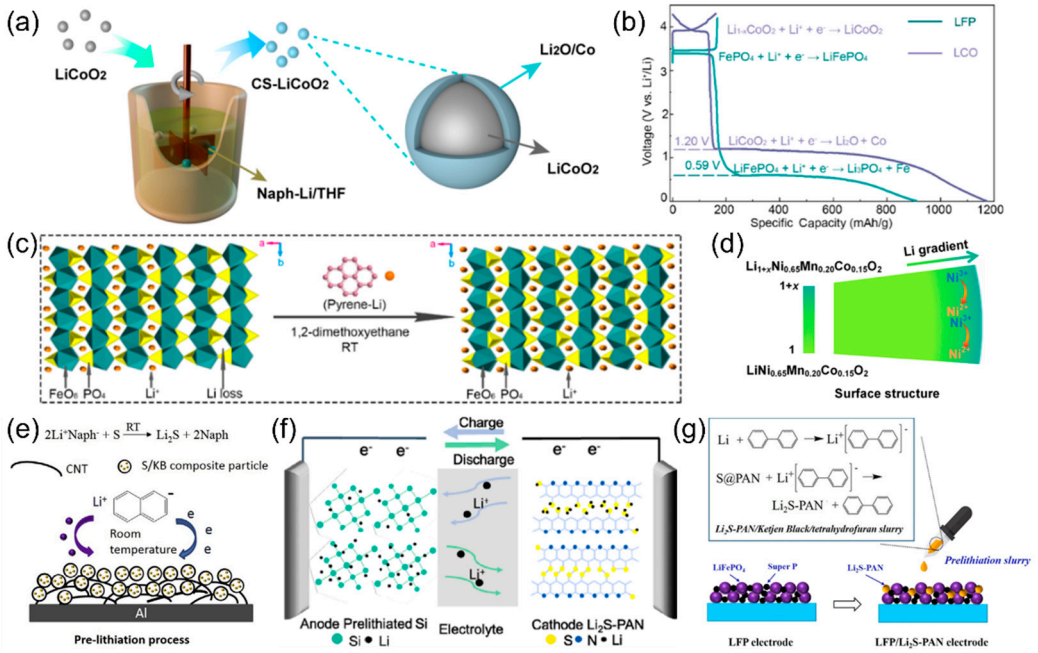

Figure 7. (**a**) Schematic illustration showing the preparation of $LiCoO_2$ cathode material with the conformal Li_2O/Co nanoshell. Reproduced with permission from ref. [47]. Copyright 2020, ACS Publications. (**b**) Charge–discharge profiles of LFP and LCO cathodes and corresponding lithiation reaction. (**c**) Schematic illustration showing the chemical relithiation for recycling the spent LFP cathode. Reproduced with permission from ref. [52]. Copyright 2021, ACS Publications. (**d**) The lithium-enriched gradient interphase structure after prelithiation. Reproduced with permission from ref. [50]. Copyright 2020, ACS Publications. (**e**) Schematic illustration showing the prelithiation of sulfur cathode by the Li-Naph complex solution. Reproduced with permission from ref. [74]. Copyright 2017, Elsevier. (**f**) Schematic illustration showing the prelithiatied Si and S electrodes to build a full cell. Reproduced with permission from ref. [48]. Copyright 2019, ACS Publications. (**g**) Schematic illustration showing the prelithiation reaction of Li-BP and S-PAN for LFP cathode. Reproduced with permission from ref. [46]. Copyright 2021, ACS Publications.

6. Presodiation Using PAH Complex Solutions

Similar to prelithiation, presodiation is an effective means to boost the output energy of Na-ion energy storage devices [78,79]. Table 3 summarizes the presodiated anode systems for Na-ion batteries. Basic PAH compounds such as Naph and BP were applied, paired with DME or THF as the complex solution for the presodiation [57–61]. Most studies utilized a low concentration of 0.1 M to 0.5 M for the preparation of a Na-PAH complex solution, and the improved ICE can approach 100% after 1~15 min of presodiation [59–61]. In fact, as the concentration of Na-Naph/DME increased from 3 M to 5 M, the irreversible capacity of the $Na_2Ti_6O_{13}$ anode significantly decreased (Figure 8a), demonstrating the controllability of wet chemical presodiation [57]. Sun et al. developed a solution-spraying presodiation route to enhance the ICE of hard carbon anode electrodes [58]. Unlike routine wet chemical presodiation via the immersion of electrode in a Na-PAH solution for a certain

time duration, the removal of volatile THF (b.p. = 66 °C) and low boiling point Naph (b.p. = 218 °C) was implemented by simple drying after the solution spraying process, leading to the possible recycling of the reagents (Figure 8b). No inactive residues remained in the presodiated hard carbon anode, which guarantees the high energy density of full cell [58]. The SEI was preformed after the presodiated anode was in contact with the liquid electrolyte during cell assembly [58,59,80,81]. Liu et al. used Na-BP/DME as the presodiation source to improve the ICE of high-capacity Sb anode [60]. High reversible capacity (540 mAh g^{-1}), high ICE (100%), and great capacity retention (85% over 300 cycles at 4C) were achieved in the presodiated Sb anode [60]. A chemically inert, mechanically strong, and electrically insulating NaF-rich SEI layer formed by the selective reaction between the presodiated active material and the FEC solvent in the electrolyte (Figure 8c) can contribute to the cycle stability of anode [60,82–84]. The SEI formed on the presodiated Sb shows a highly homogenous structure (Figure 8d) to resist volume expansion, outperforming that on the pristine Sb (Figure 8e) [60]. Using the PAHs-based wet chemical presodiation to improve the ICE of Na-ion batteries is still emerging and under development, and recent approaches were mostly applied to anodes. There are also considerable opportunities for Na-PAH complexes to be used in other high-capacity anodes and even cathodes in the foreseeable future.

Table 3. Summary of presodiated anode performance adopting various Na-PAH complexes.

Anode	Na-PAH Complex	Presodiation Time (min)	Reversible Capacity (mAh g^{-1})	ICE before Presodiation	ICE after Presodiation	Reference
Hard Carbon	0.5 M Na-BP/DME	1	300	71.6%	103%	[59]
Hard Carbon	0.1 M Na-Naph/THF	NA	145	67%	87%	[58]
Graphene	0.5 M Na-Naph/DME	10	≈315	≈80%	96.8%	[61]
$Na_2Ti_6O_{13}$	4 M Na-Naph/DME	10	164	65.7%	99%	[57]
Sb	0.5 M Na-BP/DME	15	540	75%	100%	[60]

NA: not applicable.

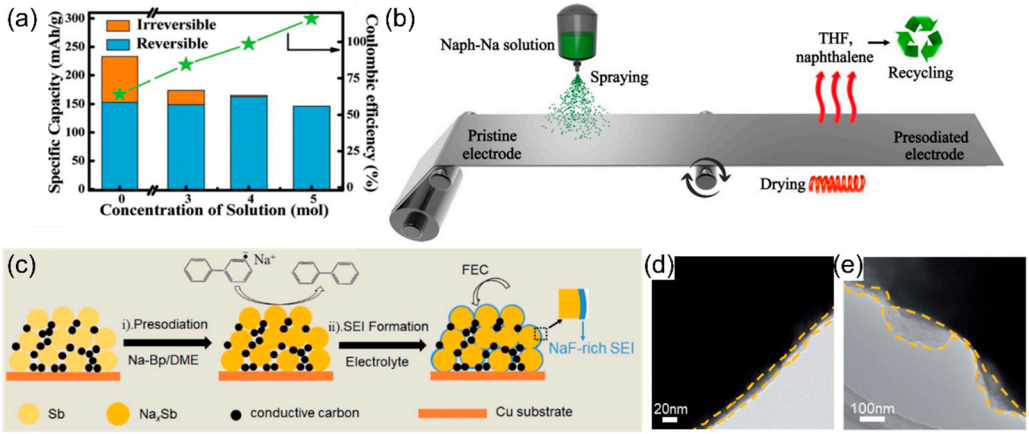

Figure 8. (**a**) Comparison of the specific capacity and Coulombic efficiency after the anode presodiation with different concentrations of the Na-Naph solution. Reproduced with permission from ref. [57]. Copyright 2019, The Royal Society of Chemistry. (**b**) Schematic illustration showing the presodiation mechanism of the hard carbon anode using a Na-Naph solution as the presodiation reagent. Reproduced with permission from ref. [58]. Copyright 2019, Wiley-VCH. (**c**) Schematic illustration showing the presodiation mechanism of the Sb anode in the Na-BP/DME solution and the subsequent SEI formation process in a Na-ion battery electrolyte (1 M $NaPF_6$ EC/DEC with 5% FEC). TEM images of the SEI layer on the (**d**) presodiated Sb and (**e**) pristine Sb anodes after one cycle. Reproduced with permission from ref. [60]. Copyright 2021, The Royal Society of Chemistry.

7. Summary and Outlook

In comparison with other methods, PAH-enabled prelithiation and presodiation show great potential to be used in Li-ion and Na-ion batteries. This scalable process is low-cost, safe, precise, uniform, efficient, and air-stable, which can facilitate the reduction in irreversible active ion loss during initial cycles and formation of an artificial protective SEI layer. Many PAH derivatives and solvent combinations have been carefully investigated, pointing out explicit guidance for different applications. The prelithiation/presodiation power and efficiency can be altered by the selections of PAH and solvents, concentration, and aging time of complex solutions. Recent studies have shown significant ICE improvements in prelithiated/presodiated anodes and cathodes for Li-ion and Na-ion batteries.

In-depth research related to the impact from the molar ratio between alkali metal and PAH molecule to the prelithiation and presodiation power and efficiency remains to be carried out in the future. Applications such as prelithiating/presodiating various electrodes for Na-ion batteries, Li-ion capacitors, and Na-ion capacitors are yet to be fully developed, leaving plenty of room for perspective research projects. Other conversion-type cathodes besides sulfur are also potential targets to be prelithiated/presodiated for high-energy-density alkali metal-free batteries.

Author Contributions: Y.-S.S. drafted the majority of this review paper. Y.-S.S. and J.-K.C. participated in discussing the contents to be included in this review paper and editing the manuscript. All authors have read and agreed to the published version of the manuscript.

Funding: This research was funded by the Ministry of Science and Technology (MOST) of Taiwan (110-2113-M-A49-027-MY2) and by the Ministry of Education (MOE) of Taiwan under the Yushan Young Scholar Program and the Higher Education SPROUT Project (111W20266) of National Yang Ming Chiao Tung University.

Data Availability Statement: All collected data are presented in the manuscript.

Conflicts of Interest: The authors declare no conflict of interest.

References

1. Li, M.; Lu, J.; Chen, Z.; Amine, K. 30 Years of Lithium-Ion Batteries. *Adv. Mater.* **2018**, *30*, 1800561. [CrossRef] [PubMed]
2. Winter, M.; Barnett, B.; Xu, K. Before Li Ion Batteries. *Chem. Rev.* **2018**, *118*, 11433–11456. [CrossRef] [PubMed]
3. Nitta, N.; Wu, F.; Lee, J.T.; Yushin, G. Li-Ion Battery Materials: Present and Future. *Mater. Today* **2015**, *18*, 252–264. [CrossRef]
4. Chayambuka, K.; Mulder, G.; Danilov, D.L.; Notten, P.H.L. From Li-Ion Batteries toward Na-Ion Chemistries: Challenges and Opportunities. *Adv. Energy Mater.* **2020**, *10*, 2001310. [CrossRef]
5. Goikolea, E.; Palomares, V.; Wang, S.; Larramendi, I.R.; Guo, X.; Wang, G.; Rojo, T. Na-Ion Batteries—Approaching Old and New Challenges. *Adv. Energy Mater.* **2020**, *10*, 2002055. [CrossRef]
6. Wu, F.; Maier, J.; Yu, Y. Guidelines and Trends for Next-Generation Rechargeable Lithium and Lithium-Ion Batteries. *Chem. Soc. Rev.* **2020**, *49*, 1569–1614. [CrossRef]
7. Guo, Y.; Li, H.; Zhai, T. Reviving Lithium-Metal Anodes for Next-Generation High-Energy Batteries. *Adv. Mater.* **2017**, *29*, 1700007. [CrossRef]
8. Choi, J.W.; Aurbach, D. Promise and Reality of Post-Lithium-Ion Batteries with High Energy Densities. *Nat. Rev. Mater.* **2016**, *1*, 16013. [CrossRef]
9. Cao, Y.; Li, M.; Lu, J.; Liu, J.; Amine, K. Bridging the Academic and Industrial Metrics for Next-Generation Practical Batteries. *Nat. Nanotechnol.* **2019**, *14*, 200–207. [CrossRef]
10. Tian, Y.; Zeng, G.; Rutt, A.; Shi, T.; Kim, H.; Wang, J.; Koettgen, J.; Sun, Y.; Ouyang, B.; Chen, T.; et al. Promises and Challenges of Next-Generation "Beyond Li-Ion" Batteries for Electric Vehicles and Grid Decarbonization. *Chem. Rev.* **2021**, *121*, 1623–1669. [CrossRef]
11. Holtstiege, F.; Bärmann, P.; Nölle, R.; Winter, M.; Placke, T. Pre-Lithiation Strategies for Rechargeable Energy Storage Technologies: Concepts, Promises and Challenges. *Batteries* **2018**, *4*, 4. [CrossRef]
12. Li, F.; Cao, Y.; Wu, W.; Wang, G.; Qu, D. Prelithiation Bridges the Gap for Developing Next-Generation Lithium-Ion Batteries/Capacitors. *Small Methods* **2022**, *6*, 2200411. [CrossRef] [PubMed]
13. Zhan, R.; Wang, X.; Chen, Z.; Seh, Z.W.; Wang, L.; Sun, Y. Promises and Challenges of the Practical Implementation of Prelithiation in Lithium-Ion Batteries. *Adv. Energy Mater.* **2021**, *11*, 2101565. [CrossRef]
14. Zou, K.; Deng, W.; Cai, P.; Deng, X.; Wang, B.; Liu, C.; Li, J.; Hou, H.; Zou, G.; Ji, X. Prelithiation/Presodiation Techniques for Advanced Electrochemical Energy Storage Systems: Concepts, Applications, and Perspectives. *Adv. Funct. Mater.* **2021**, *31*, 2005581. [CrossRef]

15. Verma, P.; Maire, P.; Novák, P. A Review of the Features and Analyses of the Solid Electrolyte Interphase in Li-Ion Batteries. *Electrochim. Acta* **2010**, *55*, 6332–6341. [CrossRef]
16. An, S.J.; Li, J.; Daniel, C.; Mohanty, D.; Nagpure, S.; Wood, D.L. The State of Understanding of the Lithium-Ion-Battery Graphite Solid Electrolyte Interphase (SEI) and Its Relationship to Formation Cycling. *Carbon* **2016**, *105*, 52–76. [CrossRef]
17. Peled, E.; Menkin, S. Review—SEI: Past, Present and Future. *J. Electrochem. Soc.* **2017**, *164*, A1703–A1719. [CrossRef]
18. Kasnatscheew, J.; Evertz, M.; Streipert, B.; Wagner, R.; Klöpsch, R.; Vortmann, B.; Hahn, H.; Nowak, S.; Amereller, M.; Gentschev, A.-C.; et al. The Truth about the 1st Cycle Coulombic Efficiency of $LiNi_{1/3}$ $Co_{1/3}$ $Mn_{1/3}$ O_2 (NCM) Cathodes. *Phys. Chem. Chem. Phys.* **2016**, *18*, 3956–3965. [CrossRef]
19. Jarvis, C.R.; Lain, M.J.; Gao, Y.; Yakovleva, M. A Lithium Ion Cell Containing a Non-Lithiated Cathode. *J. Power Sources* **2005**, *146*, 331–334. [CrossRef]
20. Jarvis, C.R.; Lain, M.J.; Yakovleva, M.V.; Gao, Y. A Prelithiated Carbon Anode for Lithium-Ion Battery Applications. *J. Power Sources* **2006**, *162*, 800–802. [CrossRef]
21. Xiang, B.; Wang, L.; Liu, G.; Minor, A.M. Electromechanical Probing of Li/Li $_2$ CO $_3$ Core/Shell Particles in a TEM. *J. Electrochem. Soc.* **2013**, *160*, A415–A419. [CrossRef]
22. Wang, F.; Wang, B.; Li, J.; Wang, B.; Zhou, Y.; Wang, D.; Liu, H.; Dou, S. Prelithiation: A Crucial Strategy for Boosting the Practical Application of Next-Generation Lithium Ion Battery. *ACS Nano* **2021**, *15*, 2197–2218. [CrossRef] [PubMed]
23. Sun, C.; Zhang, X.; Li, C.; Wang, K.; Sun, X.; Ma, Y. Recent Advances in Prelithiation Materials and Approaches for Lithium-Ion Batteries and Capacitors. *Energy Storage Mater.* **2020**, *32*, 497–516. [CrossRef]
24. Jin, L.; Shen, C.; Shellikeri, A.; Wu, Q.; Zheng, J.; Andrei, P.; Zhang, J.-G.; Zheng, J.P. Progress and Perspectives on Pre-Lithiation Technologies for Lithium Ion Capacitors. *Energy Environ. Sci.* **2020**, *13*, 2341–2362. [CrossRef]
25. Kim, H.J.; Choi, S.; Lee, S.J.; Seo, M.W.; Lee, J.G.; Deniz, E.; Lee, Y.J.; Kim, E.K.; Choi, J.W. Controlled Prelithiation of Silicon Monoxide for High Performance Lithium-Ion Rechargeable Full Cells. *Nano Lett.* **2016**, *16*, 282–288. [CrossRef]
26. Liu, W.; Chen, X.; Zhang, C.; Xu, H.; Sun, X.; Zheng, Y.; Yu, Y.; Li, S.; Huang, Y.; Li, J. Gassing in Sn-Anode Sodium-Ion Batteries and Its Remedy by Metallurgically Prealloying Na. *ACS Appl. Mater. Interfaces* **2019**, *11*, 23207–23212. [CrossRef]
27. Xu, H.; Li, S.; Zhang, C.; Chen, X.; Liu, W.; Zheng, Y.; Xie, Y.; Huang, Y.; Li, J. Roll-to-Roll Prelithiation of Sn Foil Anode Suppresses Gassing and Enables Stable Full-Cell Cycling of Lithium Ion Batteries. *Energy Environ. Sci.* **2019**, *12*, 2991–3000. [CrossRef]
28. Xu, H.; Li, S.; Chen, X.; Zhang, C.; Liu, W.; Fan, H.; Yu, Y.; Huang, Y.; Li, J. Sn-Alloy Foil Electrode with Mechanical Prelithiation: Full-Cell Performance up to 200 Cycles. *Adv. Energy Mater.* **2019**, *9*, 1902150. [CrossRef]
29. Fan, H.; Chen, B.; Li, S.; Yu, Y.; Xu, H.; Jiang, M.; Huang, Y.; Li, J. Nanocrystalline Li–Al–Mn–Si Foil as Reversible Li Host: Electronic Percolation and Electrochemical Cycling Stability. *Nano Lett.* **2020**, *20*, 896–904. [CrossRef]
30. Yu, Y.; Li, S.; Fan, H.; Xu, H.; Jiang, M.; Huang, Y.; Li, J. Optimal Annealing of Al Foil Anode for Prelithiation and Full-Cell Cycling in Li-Ion Battery: The Role of Grain Boundaries in Lithiation/Delithiation Ductility. *Nano Energy* **2020**, *67*, 104274. [CrossRef]
31. Xu, H.; Li, S.; Chen, X.; Zhang, C.; Tang, Z.; Fan, H.; Yu, Y.; Liu, W.; Liang, N.; Huang, Y.; et al. Surpassing Lithium Metal Rechargeable Batteries with Self-Supporting Li–Sn–Sb Foil Anode. *Nano Energy* **2020**, *74*, 104815. [CrossRef]
32. Jang, J.; Kang, I.; Choi, J.; Jeong, H.; Yi, K.; Hong, J.; Lee, M. Molecularly Tailored Lithium–Arene Complex Enables Chemical Prelithiation of High-Capacity Lithium-Ion Battery Anodes. *Angew. Chem. Int. Ed.* **2020**, *59*, 14473–14480. [CrossRef] [PubMed]
33. Zhang, X.; Qu, H.; Ji, W.; Zheng, D.; Ding, T.; Qiu, D.; Qu, D. An Electrode-Level Prelithiation of SiO Anodes with Organolithium Compounds for Lithium-Ion Batteries. *J. Power Sources* **2020**, *478*, 229067. [CrossRef]
34. Scott, M.G.; Whitehead, A.H.; Owen, J.R. Chemical Formation of a Solid Electrolyte Interface on the Carbon Electrode of a Li-Ion Cell. *J. Electrochem. Soc.* **1998**, *145*, 1506–1510. [CrossRef]
35. Peramunage, D.; Abraham, K.M. Preparation and Electrochemical Characterization of Overlithiated Spinel $LiMn_2$ O_4. *J. Electrochem. Soc.* **1998**, *145*, 1131–1136. [CrossRef]
36. Tabuchi, T.; Yasuda, H.; Yamachi, M. Li-Doping Process for LixSiO-Negative Active Material Synthesized by Chemical Method for Lithium-Ion Cells. *J. Power Sources* **2005**, *146*, 507–509. [CrossRef]
37. Tabuchi, T.; Yasuda, H.; Yamachi, M. Mechanism of Li-Doping into $Li_4Ti_5O_{12}$ Negative Active Material for Li-Ion Cells by New Chemical Method. *J. Power Sources* **2006**, *162*, 813–817. [CrossRef]
38. Liu, N.; Li, H.; Jiang, J.; Huang, X.; Chen, L. Li−Biphenyl−1,2-Dimethoxyethane Solution: Calculation and Its Application. *J. Phys. Chem. B* **2006**, *110*, 10341–10347. [CrossRef]
39. Holy, N.L. Reactions of the Radical Anions and Dianions of Aromatic Hydrocarbons. *Chem. Rev.* **1974**, *74*, 243–277. [CrossRef]
40. Huang, Y.; Liu, C.; Wei, F.; Wang, G.; Xiao, L.; Lu, J.; Zhuang, L. Chemical Prelithiation of Al for Use as an Ambient Air Compatible and Polysulfide Resistant Anode for Li-Ion/S Batteries. *J. Mater. Chem. A* **2020**, *8*, 18715–18720. [CrossRef]
41. Shen, Y.; Qian, J.; Yang, H.; Zhong, F.; Ai, X. Chemically Prelithiated Hard-Carbon Anode for High Power and High Capacity Li-Ion Batteries. *Small* **2020**, *16*, 1907602. [CrossRef] [PubMed]
42. Li, F.; Wang, G.; Zheng, D.; Zhang, X.; Abegglen, C.J.; Qu, H.; Qu, D. Controlled Prelithiation of SnO_2/C Nanocomposite Anodes for Building Full Lithium-Ion Batteries. *ACS Appl. Mater. Interfaces* **2020**, *12*, 19423–19430. [CrossRef] [PubMed]
43. Yan, M.-Y.; Li, G.; Zhang, J.; Tian, Y.-F.; Yin, Y.-X.; Zhang, C.-J.; Jiang, K.-C.; Xu, Q.; Li, H.-L.; Guo, Y.-G. Enabling SiO_x/C Anode with High Initial Coulombic Efficiency through a Chemical Pre-Lithiation Strategy for High-Energy-Density Lithium-Ion Batteries. *ACS Appl. Mater. Interfaces* **2020**, *12*, 27202–27209. [CrossRef] [PubMed]

44. Zhang, X.; Qu, H.; Ji, W.; Zheng, D.; Ding, T.; Abegglen, C.; Qiu, D.; Qu, D. Fast and Controllable Prelithiation of Hard Carbon Anodes for Lithium-Ion Batteries. *ACS Appl. Mater. Interfaces* **2020**, *12*, 11589–11599. [CrossRef]
45. Wang, G.; Li, F.; Liu, D.; Zheng, D.; Abeggien, C.J.; Luo, Y.; Yang, X.-Q.; Ding, T.; Qu, D. High Performance Lithium-Ion and Lithium–Sulfur Batteries Using Prelithiated Phosphorus/Carbon Composite Anode. *Energy Storage Mater.* **2020**, *24*, 147–152. [CrossRef]
46. Liu, Z.; Ma, S.; Mu, X.; Li, R.; Yin, G.; Zuo, P. A Scalable Cathode Chemical Prelithiation Strategy for Advanced Silicon-Based Lithium Ion Full Batteries. *ACS Appl. Mater. Interfaces* **2021**, *13*, 11985–11994. [CrossRef]
47. Liu, X.; Tan, Y.; Wang, W.; Li, C.; Seh, Z.W.; Wang, L.; Sun, Y. Conformal Prelithiation Nanoshell on $LiCoO_2$ Enabling High-Energy Lithium-Ion Batteries. *Nano Lett.* **2020**, *20*, 4558–4565. [CrossRef]
48. Shen, Y.; Zhang, J.; Pu, Y.; Wang, H.; Wang, B.; Qian, J.; Cao, Y.; Zhong, F.; Ai, X.; Yang, H. Effective Chemical Prelithiation Strategy for Building a Silicon/Sulfur Li-Ion Battery. *ACS Energy Lett.* **2019**, *4*, 1717–1724. [CrossRef]
49. Ren, Y.X.; Wei, L.; Jiang, H.R.; Zhao, C.; Zhao, T.S. On-Site Fluorination for Enhancing Utilization of Lithium in a Lithium–Sulfur Full Battery. *ACS Appl. Mater. Interfaces* **2020**, *12*, 53860–53868. [CrossRef]
50. Liu, X.; Liu, T.; Wang, R.; Cai, Z.; Wang, W.; Yuan, Y.; Shahbazian-Yassar, R.; Li, X.; Wang, S.; Hu, E.; et al. Prelithiated Li-Enriched Gradient Interphase toward Practical High-Energy NMC–Silicon Full Cell. *ACS Energy Lett.* **2021**, *6*, 320–328. [CrossRef]
51. Lin, L.; Qin, K.; Li, M.; Hu, Y.; Li, H.; Huang, X.; Chen, L.; Suo, L. Spinel-Related $Li_2Ni_{0.5}Mn_{1.5}O_4$ Cathode for 5-V Anode-Free Lithium Metal Batteries. *Energy Storage Mater.* **2022**, *45*, 821–827. [CrossRef]
52. Wu, C.; Hu, J.; Ye, L.; Su, Z.; Fang, X.; Zhu, X.; Zhuang, L.; Ai, X.; Yang, H.; Qian, J. Direct Regeneration of Spent Li-Ion Battery Cathodes via Chemical Relithiation Reaction. *ACS Sustain. Chem. Eng.* **2021**, *9*, 16384–16393. [CrossRef]
53. Li, Y.; Qian, Y.; Zhao, Y.; Lin, N.; Qian, Y. Revealing the Interface-Rectifying Functions of a Li-Cyanonaphthalene Prelithiation System for SiO Electrode. *Sci. Bull.* **2022**, *67*, 636–645. [CrossRef]
54. Yue, H.; Zhang, S.; Feng, T.; Chen, C.; Zhou, H.; Xu, Z.; Wu, M. Understanding of the Mechanism Enables Controllable Chemical Prelithiation of Anode Materials for Lithium-Ion Batteries. *ACS Appl. Mater. Interfaces* **2021**, *13*, 53996–54004. [CrossRef] [PubMed]
55. Shen, Y.; Shen, X.; Yang, M.; Qian, J.; Cao, Y.; Yang, H.; Luo, Y.; Ai, X. Achieving Desirable Initial Coulombic Efficiencies and Full Capacity Utilization of Li-Ion Batteries by Chemical Prelithiation of Graphite Anode. *Adv. Funct. Mater.* **2021**, *31*, 2101181. [CrossRef]
56. Choi, J.; Jeong, H.; Jang, J.; Jeon, A.-R.; Kang, I.; Kwon, M.; Hong, J.; Lee, M. Weakly Solvating Solution Enables Chemical Prelithiation of Graphite–SiO_x Anodes for High-Energy Li-Ion Batteries. *J. Am. Chem. Soc.* **2021**, *143*, 9169–9176. [CrossRef]
57. Cao, Y.; Zhang, T.; Zhong, X.; Zhai, T.; Li, H. A Safe, Convenient Liquid Phase Pre-Sodiation Method for Titanium-Based SIB Materials. *Chem. Commun.* **2019**, *55*, 14761–14764. [CrossRef]
58. Liu, X.; Tan, Y.; Liu, T.; Wang, W.; Li, C.; Lu, J.; Sun, Y. A Simple Electrode-Level Chemical Presodiation Route by Solution Spraying to Improve the Energy Density of Sodium-Ion Batteries. *Adv. Funct. Mater.* **2019**, *29*, 1903795. [CrossRef]
59. Liu, M.; Zhang, J.; Guo, S.; Wang, B.; Shen, Y.; Ai, X.; Yang, H.; Qian, J. Chemically Presodiated Hard Carbon Anodes with Enhanced Initial Coulombic Efficiencies for High-Energy Sodium Ion Batteries. *ACS Appl. Mater. Interfaces* **2020**, *12*, 17620–17627. [CrossRef]
60. Liu, M.; Yang, Z.; Shen, Y.; Guo, S.; Zhang, J.; Ai, X.; Yang, H.; Qian, J. Chemically Presodiated Sb with a Fluoride-Rich Interphase as a Cycle-Stable Anode for High-Energy Sodium Ion Batteries. *J. Mater. Chem. A* **2021**, *9*, 5639–5647. [CrossRef]
61. Zheng, G.; Lin, Q.; Ma, J.; Zhang, J.; He, Y.; Tang, X.; Kang, F.; Lv, W.; Yang, Q. Ultrafast Presodiation of Graphene Anodes for High-efficiency and High-rate Sodium-Ion Storage. *InfoMat* **2021**, *3*, 1445–1454. [CrossRef]
62. Wang, G.; Li, F.; Liu, D.; Zheng, D.; Luo, Y.; Qu, D.; Ding, T.; Qu, D. Chemical Prelithiation of Negative Electrodes in Ambient Air for Advanced Lithium-Ion Batteries. *ACS Appl. Mater. Interfaces* **2019**, *11*, 8699–8703. [CrossRef] [PubMed]
63. Takeshita, T.; Hirota, N. Alkali Metal NMR Studies of Radical Anion Solutions. *J. Chem. Phys.* **1973**, *58*, 3745–3756. [CrossRef]
64. Canters, G.W.; de Boer, E.; Alkali, N.M.R. Experiments on the Radical Ion Pairs of Biphenyl and Fluorenone: Part I. Analysis of N.M.R. Shifts. *Mol. Phys.* **1973**, *26*, 1185–1198. [CrossRef]
65. Zheng, J.; Lochala, J.A.; Kwok, A.; Deng, Z.D.; Xiao, J. Research Progress towards Understanding the Unique Interfaces between Concentrated Electrolytes and Electrodes for Energy Storage Applications. *Adv. Sci.* **2017**, *4*, 1700032. [CrossRef]
66. Ming, J.; Cao, Z.; Wahyudi, W.; Li, M.; Kumar, P.; Wu, Y.; Hwang, J.-Y.; Hedhili, M.N.; Cavallo, L.; Sun, Y.-K.; et al. New Insights on Graphite Anode Stability in Rechargeable Batteries: Li Ion Coordination Structures Prevail over Solid Electrolyte Interphases. *ACS Energy Lett.* **2018**, *3*, 335–340. [CrossRef]
67. Su, Y.-S.; Hsiao, K.-C.; Sireesha, P.; Huang, J.-Y. Lithium Silicates in Anode Materials for Li-Ion and Li Metal Batteries. *Batteries* **2022**, *8*, 2. [CrossRef]
68. Yu, S.-H.; Feng, X.; Zhang, N.; Seok, J.; Abruña, H.D. Understanding Conversion-Type Electrodes for Lithium Rechargeable Batteries. *Acc. Chem. Res.* **2018**, *51*, 273–281. [CrossRef]
69. Wu, F.; Yushin, G. Conversion Cathodes for Rechargeable Lithium and Lithium-Ion Batteries. *Energy Environ. Sci.* **2017**, *10*, 435–459. [CrossRef]
70. Manthiram, A.; Fu, Y.; Chung, S.-H.; Zu, C.; Su, Y.-S. Rechargeable Lithium–Sulfur Batteries. *Chem. Rev.* **2014**, *114*, 11751–11787. [CrossRef]
71. Manthiram, A.; Fu, Y.; Su, Y.-S. Challenges and Prospects of Lithium–Sulfur Batteries. *Acc. Chem. Res.* **2013**, *46*, 1125–1134. [CrossRef] [PubMed]

72. Fu, Y.; Su, Y.-S.; Manthiram, A. Highly Reversible Lithium/Dissolved Polysulfide Batteries with Carbon Nanotube Electrodes. *Angew. Chem. Int. Ed.* **2013**, *52*, 6930–6935. [CrossRef] [PubMed]
73. Fu, Y.; Su, Y.-S.; Manthiram, A. Li_2S-Carbon Sandwiched Electrodes with Superior Performance for Lithium-Sulfur Batteries. *Adv. Energy Mater.* **2014**, *4*, 1300655. [CrossRef]
74. Wu, Y.; Momma, T.; Ahn, S.; Yokoshima, T.; Nara, H.; Osaka, T. On-Site Chemical Pre-Lithiation of S Cathode at Room Temperature on a 3D Nano-Structured Current Collector. *J. Power Sources* **2017**, *366*, 65–71. [CrossRef]
75. Fanous, J.; Wegner, M.; Grimminger, J.; Andresen, Ä.; Buchmeiser, M.R. Structure-Related Electrochemistry of Sulfur-Poly(Acrylonitrile) Composite Cathode Materials for Rechargeable Lithium Batteries. *Chem. Mater.* **2011**, *23*, 5024–5028. [CrossRef]
76. Wang, W.; Cao, Z.; Elia, G.A.; Wu, Y.; Wahyudi, W.; Abou-Hamad, E.; Emwas, A.-H.; Cavallo, L.; Li, L.-J.; Ming, J. Recognizing the Mechanism of Sulfurized Polyacrylonitrile Cathode Materials for Li–S Batteries and beyond in Al–S Batteries. *ACS Energy Lett.* **2018**, *3*, 2899–2907. [CrossRef]
77. Warneke, S.; Hintennach, A.; Buchmeiser, M.R. Communication—Influence of Carbonate-Based Electrolyte Composition on Cell Performance of SPAN-Based Lithium-Sulfur-Batteries. *J. Electrochem. Soc.* **2018**, *165*, A2093–A2095. [CrossRef]
78. Zhang, M.; Li, Y.; Wu, F.; Bai, Y.; Wu, C. Boost Sodium-Ion Batteries to Commercialization: Strategies to Enhance Initial Coulombic Efficiency of Hard Carbon Anode. *Nano Energy* **2021**, *82*, 105738. [CrossRef]
79. Chojnacka, A.; Pan, X.; Bachetzky, C.; Brunner, E.; Béguin, F. A Strategy for Optimizing the Output Energy and Durability of Metal-Ion Capacitors Fabricated with Alloy-Based Anodes. *Energy Storage Mater.* **2022**, *51*, 719–732. [CrossRef]
80. Rodriguez, R.; Loeffler, K.E.; Nathan, S.S.; Sheavly, J.K.; Dolocan, A.; Heller, A.; Mullins, C.B. In Situ Optical Imaging of Sodium Electrodeposition: Effects of Fluoroethylene Carbonate. *ACS Energy Lett.* **2017**, *2*, 2051–2057. [CrossRef]
81. Zheng, J.; Zhang, H.; Dong, S.; Liu, Y.; Tai Nai, C.; Suk Shin, H.; Young Jeong, H.; Liu, B.; Ping Loh, K. High Yield Exfoliation of Two-Dimensional Chalcogenides Using Sodium Naphthalenide. *Nat. Commun.* **2014**, *5*, 2995. [CrossRef] [PubMed]
82. Ji, L.; Gu, M.; Shao, Y.; Li, X.; Engelhard, M.H.; Arey, B.W.; Wang, W.; Nie, Z.; Xiao, J.; Wang, C.; et al. Controlling SEI Formation on SnSb-Porous Carbon Nanofibers for Improved Na Ion Storage. *Adv. Mater.* **2014**, *26*, 2901–2908. [CrossRef]
83. Yildirim, H.; Kinaci, A.; Chan, M.K.Y.; Greeley, J.P. First-Principles Analysis of Defect Thermodynamics and Ion Transport in Inorganic SEI Compounds: LiF and NaF. *ACS Appl. Mater. Interfaces* **2015**, *7*, 18985–18996. [CrossRef] [PubMed]
84. Fang, W.; Jiang, H.; Zheng, Y.; Zheng, H.; Liang, X.; Sun, Y.; Chen, C.; Xiang, H. A Bilayer Interface Formed in High Concentration Electrolyte with SbF_3 Additive for Long-Cycle and High-Rate Sodium Metal Battery. *J. Power Sources* **2020**, *455*, 227956. [CrossRef]